nature communications

Article

https://doi.org/10.1038/s41467-025-58996-9

Engineering coupled consortia-based biosensors for diagnostic

Received: 4 March 2024

Accepted: 9 April 2025

Published online: 22 April 2025

Check for updates

Rongying Huang[1], Valeriia Kravchik[2], Rawan Zaatry[3], Mouna Habib[2], Naama Geva-Zatorsky[3,4] & Ramez Daniel[2]

Synthetic multicellular systems have great potential for performing complex tasks, including multi-signal detection and computation through cell-to-cell communication. However, engineering these systems is challenging, requiring precise control over the cell concentrations of distinct members and coordination of their activity. Here, we develop a bacterial consortia-based biosensor for Heme and Lactate, wherein members are coupled through a global shared quorum-sensing signal that simultaneously controls the activity of the diverse biosensing strains. The multicellular system incorporates a gene circuit that computes the minimum between each biosensor's activity and the shared signal. We evaluate three consortia configurations: one where the shared signal is externally supplied, another directly produced via an inducible gene circuit, and a third generated through an incoherent feedforward loop (IFFL) gene circuit. Among these configurations, the IFFL system, which maintains the shared signal at low and stable levels over an extended period, demonstrates improved performance and robustness against perturbations in cell populations. Finally, we examine these coupled consortia to monitor Lactate and Heme in humanized fecal samples for diagnostics.

Engineered multicellular systems harness the diverse abilities of individual populations, enabling cooperative interactions to accomplish complex tasks across various applications, including bioproduction[1], healthcare[2], and environmental monitoring[3]. For instance, synthetic consortia have been developed to address challenges in bacterial biosensor performance, including enhancing multi-target detection[4] and minimizing crosstalk between analytes[5,6]. These tasks often require large-scale gene circuits, which, when carried out by a single strain, can impose a burden on gene expression and deplete vital resources[7,8]. Moreover, bacterial biosensors often undergo genetic modifications, such as removing essential genes or adding genes to improve sensing sensitivity[9]. However, combining these modifications within a single strain can result in crosstalk among diverse biological processes[10]. By distributing complex genetic pathways across multiple species, synthetic consortia can alleviate this burden, enhancing overall functionality and reducing strain-specific limitations[6,11].

Despite significant progress in engineering synthetic microbial consortia, further advancements in their design are still required[12]. In synthetic consortia, individual members are often uncoupled and function independently within the network[13], leading to challenges such as output misinterpretation[14], as the observed output is influenced not only by the intended activity of each member (f_i) but also by their cell concentrations (N_i) ($Out \propto \sum_{i=1}^{M} N_i \cdot f_i$) (Fig. 1a) ('Analog Signal Control in Biosensor Consortia' section in Methods). Proper operation of uncoupled consortia requires maintaining a balance in the cell concentrations of the different members over time—a task that becomes increasingly challenging in complex environments[15]. In contrast, coupled consortia, meaning each member is aware of the presence and activity of the others, an optimized design can be

[1]Department of Biotechnology Technion—Israel Institute of Technology, Technion City, Haifa, Israel. [2]Department of Biomedical Engineering Technion—Israel Institute of Technology, Technion City, Haifa, Israel. [3]Department of Cell Biology and Cancer Science, Rappaport Technion Integrated Cancer Center (RTICC), Rappaport Faculty of Medicine, Technion – Israel Institute of Technology, 3525422 Haifa, Israel. [4]CIFAR, MaRS Centre, West Tower 661 University Avenue, Suite 505, Toronto, ON M5G 1M1, Canada. e-mail: ramizda@bm.technion.ac.il

https://doi.org/10.1038/s41467-025-58996-9

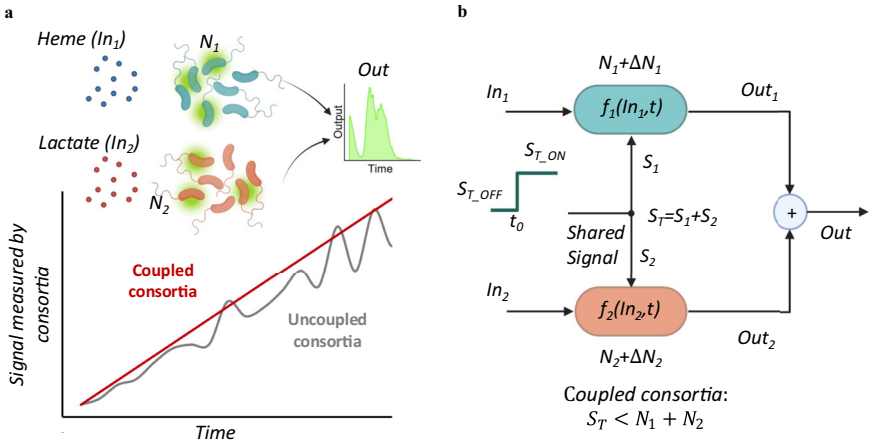

Fig. 1 | Coupled biosensors through shared signaling molecules. a Different biomarker inputs (In_1 and In_2 represent the Heme and Lactate in our study) trigger two bacterial biosensor consortia, each with its own cell concentration (N_1 and N_2). When the system is activated by the input signals (In_1 and In_1), only part of N_1 and N_2 (indicated in green color) contribute to the overall output (*Out*). The red and gray curves are illustrative and used to represent the effects of input coupling within the consortia. The coupling consortia (red curve) is shown to enhance the robustness and reliability of the output compared to the uncoupled consortia (gray curve). These curves do not depict actual experimental responses. **b** A coupled consortia ($S_T < N1 + N2$) with shared signaling molecules (S_T represents CHL in this study) that is distributed across the entire consortia $S_T = S_1 + S_2$. This shared signal controls the activity of two different bacterial biosensors ($f_1(In_1, t)$ and $f_2(In_2, t)$ represent the activities of Heme and Lactate in our study. Under changes in the cell concentration (N1 + ΔN1 and N2 + ΔN2), this coupled consortium consortia shows a more robust output ($Out = Out_1 + Out_2$) compared to an uncoupled consortium. Figures created with BioRender.

achieved[4,11,16–19]. Such consortia, where members are linked and their activities are coordinated, could exhibit reduced dependency on individual cell concentrations, resulting in more robust system performance against the perturbations of cell concentration ('Mathematical Modelling for Signal Coupling in Microbial Consortia' in Methods)[20].

Coupled consortia can be established using either a negative feedback loop to maintain cell concentrations at specific levels[21] or through indirect interactions where cells compete for a shared activation source (Fig. 1a)[22]. In this study, we focused on indirect interactions by simultaneously activating the different biosensors within the consortia using shared signaling molecules (S_T). Coupling among consortia members occurs when the concentration of the shared signaling molecule is lower than the total cell population ($S_T < \sum_{i=1}^{M} N_i$), ensuring the activity of the consortia members is governed by the availability of the shared signal rather than their population size. In this scenario, the shared signal acts as a limiting factor for activation of the various biosensor strains, rather than the cell density. This coupling, in turn, minimizes the impact of fluctuations and perturbations in individual member cell concentrations on the overall consortia's output (Fig. 1b and the section 'Mathematical Modelling for Signal Coupling in Microbial Consortia' in Materials and Methods). Furthermore, when the shared signal is inducible, it functions as an enabling signal for the consortium-based biosensor[23], allowing signal transmission when the external inducer is high and blocking transmission when the inducer is low.

For biological systems with an analog response, such as bacterial biosensors, the enable signal's mechanism can be implemented by a genetic circuit that computes the minimum (MIN) between the shared signaling molecules (S_T) and the biosensor response activity (Supplementary Fig. 1 and 'Designing and Modeling of a Bioluminescent *luxCDABE* Cassette' in Supplementary Methods). In this design (Fig. 1b), where S_T simultaneously facilitates coupling and enabling between consortia members, programming its appropriate ON and OFF levels (S_{T_ON} and S_{T_OFF}) presents a significant challenge. The concentration of these molecules must be lower than the total cell concentration to couple the cells effectively, yet higher than the activity of each biosensor to accurately compute the minimum operation (Eq. 19 and the section 'Analog Signal Control in Biosensor Consortia' in Methods). To address this challenge, we implemented an incoherent type-1 feed-forward loop (IFFL) to regulate the synthesis of the shared signal due to the network's ability to maintain the signal stable at low levels for an extended period, e.g., spanning >15 h in laboratory condition (LB medium). In the IFFL circuit, the input simultaneously activates and, through an intermediary molecule, inhibits the output protein, either a reporter protein or catalyst for synthesizing quorum-sensing (QS) signals that serve as shared signals ('Conceptual and Mathematical Examination of the IFFL Network Dynamics' in Methods)[24–28]. The IFFL circuit generates a shared signal that efficiently manages biosensor information, coupling the activities of bacterial consortia and integrating diverse cellular data, thereby ensuring the functionality of the collective system.

This study involves three consortia configurations for simultaneously detecting Heme and Lactate (Fig. 1b). The first configuration, termed the "IFFL Network System," consists of three strains: two strains dedicated to detecting the Heme and Lactate biomarkers, respectively and a third strain responsible for producing the QS shared signal at low levels via an IFFL network. The second configuration, termed the "Direct Regulation System," is similar to the first, but the shared signal is generated at high levels through a transcriptional cascade of two layers. Both configurations generate the shared CHL signal, but their underlying network architectures differ. Finally, the third configuration, termed the "External Induction System," consists of Heme and Lactate bacterial biosensors where the shared signal is externally supplied once. The purpose of this configuration is to compare the effects of signal production by a bacterial strain with the direct external addition of the shared signal on the consortia output. Additionally, it enables an assessment of how different concentrations of the shared signal influence system performance. Heme is associated with bleeding[29,30], often accompanied by unhealthy conditions such as inflammatory bowel disease (IBD), various types of colitis (e.g., ischemic colitis, infectious colitis), and neoplasia[31]. Lactate is associated with IBD[32,33], colorectal cancer (CRC)[34,35], and lactic acidosis[34]. Both molecules can be identified in the feces of patients experiencing inflammation. In summary, we evaluated the performance of three synthetic consortia for

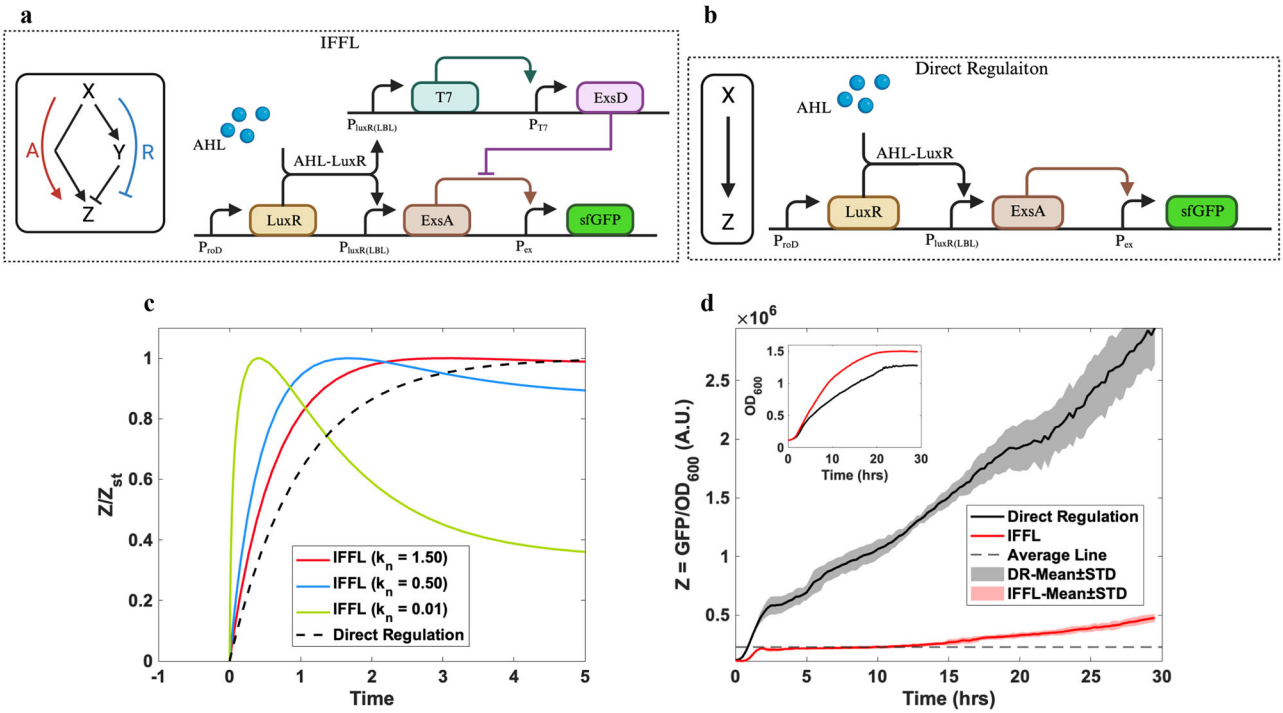

Fig. 2 | Development of Incoherent Type-1 Feedforward Loop (IFFL) circuit. **a** Schematic diagram and genetic circuit for incoherent type-1 feedforward loop (IFFL). **b** Schematic diagram and genetic circuit for direct regulation. **c** Simulation results are described the normalized Eqs. (1)–(3) (Methods). The IFFL network is represented by curves in different colors corresponding to various k_n values: $k_n = 1.5$ (red), $k_n = 0.5$ (blue), and $k_n = 0.01$ (green). The direct regulation circuit is depicted by the black dashed curve. The remaining parameters are $\alpha_0 = \alpha_1 = \gamma_1 = \rho = \gamma_0 = \gamma_2 = n = 1$ (Methods). **d** Plate reader experiments show the dynamics for the IFFL network and direct regulation circuit for about 30 h, represented by red and black curves, respectively. The gray dashed line indicates the average value of the IFFL network between 2 and 15 h. Unless further stated, the shaded area around the curve indicates the standard deviation of three replicants in the measurements and the measure of center represents the mean. The inset figure shows the optical density (OD_{600}) of cells in the IFFL network and direct regulation circuit. Source data are provided as a Source Data file. Figures **a**, **b** created with BioRender.

detecting Heme and Lactate, with the IFFL demonstrating better performance.

Results

Synthetic IFFL network

An IFFL motif (Fig. 2a) consists of three components: an initial regulator (X) that directly activates the target gene (Z) and indirectly represses it through an intermediate regulator (Y). IFFL motifs are commonly observed in natural gene networks and have been integrated into many synthetic biological systems, with a range of functionalities, including pulse generation[36,37], amplitude band-pass filtering[38,39], response time acceleration[40,41], perfect adaptation and dosage gene stability[37,42], fold change detection in input signals[43,44], and analog-to-digital data conversion[45]. In this study, we engineered the IFFL circuit to exhibit sustained plateau-like stability. To achieve such behavior, our simulation results indicate that the IFFL network (Fig. 2c) should be programmed so that the repression pathway (R) is weaker than the activation pathway (A) ('Conceptual and Mathematical Examination of the IFFL Network Dynamics' in Methods). In this specific design, called plateau-like output ($k_n = 1.50$, red curve; $k_n = 0.5$, blue curve in Fig. 2c), the initial rise in output is driven by direct activation. Subsequently, after a time delay, repression begins to compensate for the activation, resulting in a stable output and an earlier transition to a steady state. In contrast, in the pulse-like output design ($k_n = 0.01$, Fig. 2c green curve), when repression is more dominant, the signal decreases to its baseline state following the initial stimulus. Here, the k_n parameter quantifies the relative strength between the activation and repression pathways. A larger value of k_n means activation is more dominant in the process ('Conceptual and Mathematical Examination of the IFFL Network Dynamics' in Methods).

To experimentally implement such an IFFL network (Fig. 2a), we utilized genetic circuits, which are triggered by Acyl Homoserine Lactones 3OC6HSL (AHL)[46]. The AHL molecules bind to the *LuxR* activating $P_{lux(LBL)}$, a low basal level (LBL) P_{lux} promoter. This promoter is designed to lower its basal activity and extend the time required to achieve steady-state expression[45]. In turn, the $P_{lux(LBL)}$ governs two distinct pathways: *ExsA*, directly activating the super-fold green fluorescent protein fused with the ssrA degradation tag (*sfGFP*), and T7 RNA polymerase (*T7 RNAP*)[47], initiating the anti-activator *ExsD*. Specifically, we selected *ExsD* to shunt *ExsA* from binding to the P_{ex} promoter, which activates the *sfGFP* expression. In the regulatory mechanism of P. aeruginosa's Type Three Secretion System (TTSS), two proteins, *ExsA* and *ExsD*, play pivotal roles in linking transcription with secretion. *ExsA* acts as an essential transcriptional activator necessary for expressing the complete set of TTSS genes[48,49]. On the other hand, *ExsD* functions as an anti-activator to balance the activity of *ExsA*[50]. The *sfGFP* is fused with a *ssrA* degradation tag, shortening its half-life. The selection of *sfGFP-ssrA* ensures that the kinetics of the fluorescent protein would have minimized the impact on the overall response time of the genetic circuit. We also constructed a direct regulation circuit (Fig. 2b) comprising only the activation pathway (A) of the IFFL network through a two-layer genetic cascade.

We recorded the time-response characteristic (GFP/OD_{600}) of both the IFFL network and direct regulation circuit for about 30 h, each activated by the inducer AHL at the initial time (Fig. 2d). The GFP/OD_{600} measurements represent population-level data normalized per cell. An IFFL-based gene circuit can maintain the production at constant low levels for an extended period (Fig. 2d, red curve), spanning over 15 h, while direct regulation results show an increase in the GFP/OD_{600} levels over time (Fig. 2d, black curve). Using the mean value of

https://doi.org/10.1038/s41467-025-58996-9

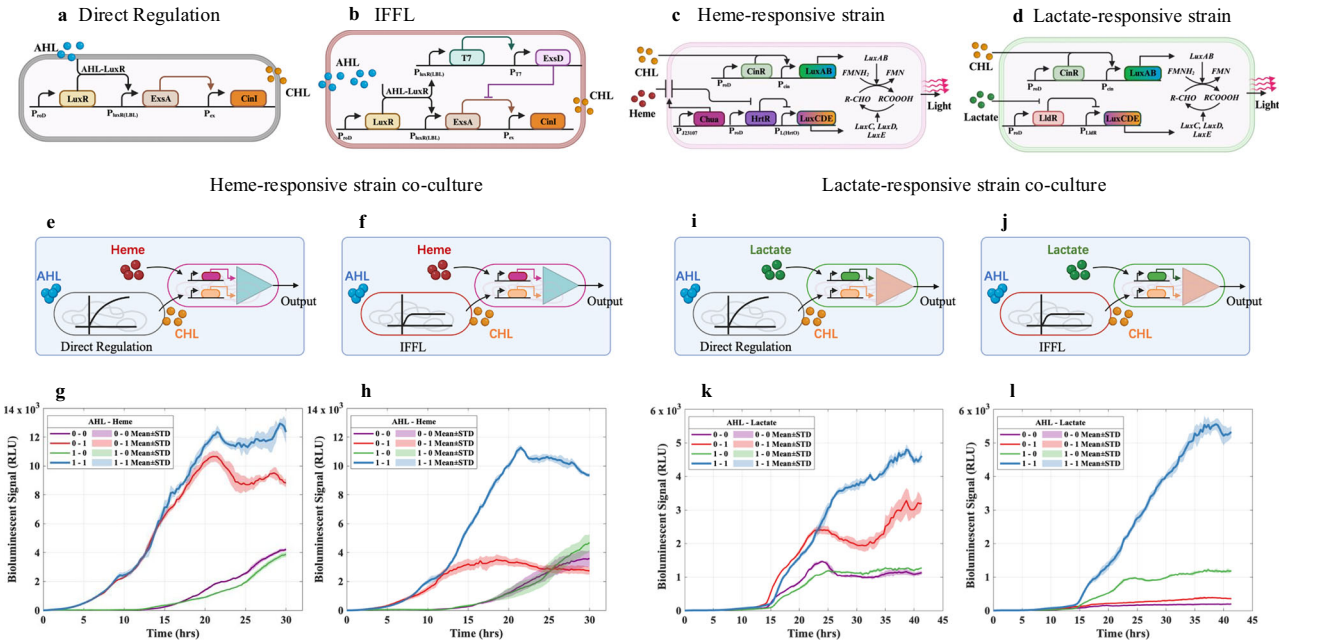

Fig. 3 | Whole-cell biosensors using Direct Regulation and IFFL network co-cultures. a–d Basic genetic circuits: (**a**) Direct regulation circuit, (**b**) Stability output IFFL network, (**c**) Heme-responsive strain, and (**d**) Lactate-responsive strain. **e–h** Dynamic responses and schematic diagram of Heme-responsive strain co-cultures with direct regulation (**e**, **g**) or IFFL network (**f**, **h**). For both consortia, the response to combinations of AHL and Heme is monitored: '00' (purple curve) signifies no inducers, '01' (red curve) indicates Heme only, '10' (green curve) represents AHL only, and '11' (blue curve) indicates the presence of both AHL and Heme. **i–l** Dynamic responses and schematic diagram of Lactate-responsive strain co-cultures. The direct regulation co-culture response to AHL and Lactate is shown in (**i**, **k**) while the IFFL network's response is in (**j**, **l**). The conditions tested are analogous to those in (**e–h**), with '00' as the no inducers, '01' for Lactate, '10' for AHL, and '11' for both inducers present. Source data are provided as a Source Data file. Figures **a–j** created with BioRender.

the IFFL experimental data curve between 2 to 15 h (Fig. 2d, vertical black dashed line), the variance between the experimental data and the average line exhibited less than a 20% fluctuation (Supplementary Fig. 2), suggesting a stable expression over this time. To compare with the simulation output (Fig. 2c), we also present the normalized signal relative to its maximum level Z/Z_{max}, demonstrating that the IFFL network achieves a steady state at least three times faster than direct regulation (Supplementary Fig. 3). Here, the response time refers to the duration required for the circuit to reach its steady state. Additionally, when we constructed a new IFFL circuit (Supplementary Fig. 4) with a different repression pathway compared to the activation pathways (i.e., k_n around 0.2), we experimentally observed a pulse-like behavior rather than a stable signal, consistent with our simulation results (Fig. 2c).

In the direct regulation circuit, we observed a consistent rise in the output over time (Fig. 2d, black curve), lasting ~30 h without reaching saturation. A simpler version of the direct regulation circuit, including a single-layer gene circuit, was also constructed and tested (Supplementary Fig. 5). Notably, the absence of the *exsA* gene in this circuit did not accelerate the process of reaching a steady state. When the circuit was induced with a low AHL concentration (3 nM), it reached a steady state after 13 h. This suggests that lowering the AHL concentration may help accelerate the steady-state process in the direct regulation system. However, this simpler direct regulation circuit presents challenges as the P_{lux} promoter does not operate at its ON binary level[44], making the system highly sensitive to AHL fluctuations (Supplementary Fig. 6).

Comparing the growth rates (OD_{600}) of cells from the IFFL network and direct regulation circuit, the IFFL network reaches a higher cell concentration (Fig. 2d, inset). This result suggests that the IFFL network utilizes fewer resources in the same environment and potentially performs better in resource-limited settings. Moreover, the dynamic response of the IFFL circuit demonstrates reduced stability after 15 h as the cells enter the stationary phase ($OD_{600} > 1$, Supplementary Fig. 7). To validate this, we conducted experiments (Supplementary Figs. 8–10) that maintained the OD_{600} of the IFFL network and direct regulation circuit in their exponential growth phase for an extended period of ~24.5 h (Supplementary Fig. 8). These results indicated that the IFFL circuit exhibited stability over this extended period (Supplementary Figs. 8–9). Finally, we tested both circuits in M9 media supplemented with 0.4% glucose, where they reached the stationary phase earlier than in LB, resulting in shorter stability period compared to in LB media(Supplementary Fig. 10).

Whole-cell biosensors

The IFFL network demonstrated long-term (e.g., a couple of days) stability and low output expression, making it ideally suited to serve as a signal for cohesively integrating the activity of biosensors within consortia. According to our model (Eq. 19 in section 'Mathematical Modelling for Signal Coupling in Microbial Consortia' in Methods), when the concentration of the shared signal is lower than the total cell concentration, a coupling between the cells is established. Furthermore, maintaining a consistent signal over time across multiple bacterial biosensors ensures a uniform impact of the shared signal on their output.

To evaluate the stability signal with the bacterial biosensors, we created four strains: two of these strains are activated by AHL and produce an orthogonal QS cell-cell signaling molecule acyl-homoserine lactone 3OHC14:1-HSL (CHL), one through direct regulation (Fig. 3a) and the other through IFFL network (Fig. 3b). For both strains, we replaced the sfGFP, as shown in Fig. 2a, b, with *CinI* (Fig. 3a, b). The *CinI* serves as an enzyme responsible for catalyzing the synthesis of CHL, which then distributes throughout the media and diffuses into the consortia wiring Heme and Lactate-responsive biosensor strain's activities (Fig. 3). The CHL molecule functions as a shared signal to couple the other members within the consortia. The

third and fourth strains include a genetic circuit that computes a minimum operation ('Designing and Modeling of a Bioluminescent luxCDABE Cassett' in Supplementary Methods) between the responses of CHL and either Heme (Fig. 3c) or Lactate (Fig. 3d). The minimum operation circuit was implemented by reengineering the bioluminescent *luxCDABE* reporter[49]. In this system, the *luxAB* genes, encoding the luciferase subunits responsible for catalyzing the luminescence reaction, are regulated by the CHL, while the *luxCDE* genes, encoding the fatty acid reductase complex required for synthesizing the fatty aldehyde substrate, are controlled by either the Heme- or Lactate-responsive pathways[51]. When the *luxAB* and *luxCDE* are divided and regulated by two distinct inputs, the bioluminescent signal (I) is described by $I \propto MIN\left\{\frac{g(LuxAB)}{K_R}, \frac{h(luxCDE)}{K_F}\right\}$, where g is a function of LuxA and LuxB concentrations, h is a function of LuxC, LuxD, and LuxE concentrations, and K_R and K_F are the reverse and forward rates of the bioluminescent reaction ('Designing and Modeling of a Bioluminescent luxCDABE Cassett' in Supplementary Methods), respectively[52]. Notably, the minimum operation (MIN) functions as an AND logic gate when applied to binary inputs [0,1]. For example, when both the CHL and Heme or Lactate-responsive pathways are activated, then the system would go into the 'ON' state. In contrast, it remains an 'OFF' state when only one or none of the pathways is activated (Supplementary Fig. 11). For the Heme-responsive strain, the Lactococcus lactis Heme-responsive transcriptional repressor *HrtR* and an outer-membrane transporter *ChuA* are expressed under constitutive promoters P_{roD} and P_{J23107}, respectively, which are located on an MCP. Extracellular Heme enters bacterial cells through the outer-membrane transporter *ChuA* and interacts with the transcriptional repressor *HrtR* to allow for the expression of *LuxCDE* genes. The Heme input regulates *luxCDE* genes via the Heme-sensitive promoter $P_{L(HrtO)}$, which is located on an HCP. For the Lactate-responsive strain, the CHL-responsive pathway is the same as the Heme-responsive strain, which is also located on LCP. The Lactate-responsive pathway contains the constitutive production (P_{rod}) of an *LldR* repressor, which is located on MCP. Transcriptional regulation in *E. coli* in response to Lactate involves the Lactate-sensing transcription factor *LldR*, a member of the *GntR* family. *LldR* is capable of sensing Lactate[53]. It derepresses the P_{LldR} promoter and activates the expression of *LuxCDE* in the presence of Lactate, located on the HCP.

Next, we explored the dynamic interaction between the two strains in a co-culture environment. For Heme-responsive strain co-culture (Fig. 3e, f); either the direct regulation circuit (Fig. 3a) or the stability output IFFL network (Fig. 3b) was combined with the Heme-responsive strain (Fig. 3c) at a chosen 1:1 ratio in volume. The experiments were conducted with AHL at a concentration of 2 μM and Heme at 2 μM. This Heme concentration approaches the range where the Heme-biosensor reaches its maximum activity. (Supplementary Fig. 12). Then, we introduced the AHL and Heme inducers into the system in four distinct states: without any inducers ('00'), with Heme alone ('01'), with AHL alone ('10'), and with both Heme and AHL present ('11'), to assess the consortia's functionality. The output representation of the systems developed in this study was evaluated using bioluminescent signals, as OD_{600} measurements are often impractical in real-world biosensing applications. Unless specified otherwise, bioluminescent signals are used to represent the output throughout the following sections.

For both co-cultures, the '00' state (Fig. 3g, h, purple curve) remains at a low level, indicating minimal background activity without inducers ('OFF' state). The '10' state (Fig. 3g, h, green curve), representing the presence of AHL only, shows a similar response compared to the '00' state in bioluminescence. For the direct regulation co-culture (Fig. 3g), the '11' state demonstrates the highest bioluminescence level, suggesting an additive effect of the inducers. However, the '01' state, which represents the presence of Heme only, displays a response similar to the '11' state in both shape and signal intensity, indicating that Heme alone can elicit a response nearly equivalent to that of both inducers combined[50–52]. These results indicate that the direct regulation co-cultures cannot distinguish between the '11' and '10' states. This limitation is likely due to the high background levels of CHL produced within the consortia (Supplementary Table 1) despite using a promoter with inherently low basal activity to regulate CHL synthesis. The decline in signal (after 20 h) intensity over time is primarily attributed to the consumption or degradation of Heme[54–56].

Compared to the direct regulation and Heme-responsive strain co-cultures (Fig. 3e and g), the IFFL strain co-culture (Fig. 3f and h) exhibits a more moderated response for the '01' state and a significantly lower signal than the '11' state. Consequently, the '11' state can be distinctly differentiated from other states (Fig. 3h). These results confirm the capability of the stable IFFL output signal to control the temporal progression of the input signals. To quantify the CHL concentration produced by the direct regulation circuit (Fig. 3a) and the IFFL network (Fig. 3b), we compared their dynamic response at the final time points (around 20 h) to the one of a Heme-responsive strain induced with 2 μM of Heme and with various concentrations of CHL (Supplementary Fig. 13). For direct regulation circuit (Supplementary Fig. 13A), the '11' state, acting as 'ON' state, corresponds to the response of the Heme-responsive strain at 0.5 μM CHL, while the '01' state, acting as 'OFF' state, corresponds to 0.125 μM CHL. For the IFFL network (Supplementary Fig. 13B), the 'ON' and 'OFF' states correspond to ~0.125 μM and <0.03 μM, respectively. The OD_{600} signals show a similar continuous increase across different states. This consistency suggests that observed differences in output signals are primarily due to the circuits' behavior rather than variations in growth rate (Supplementary Fig. 14). The OD_{600} measurement spans both the exponential and stationary phases of growth. Unless otherwise specified, OD_{600} measurements were provided throughout the subsequent sections to ensure clarity and reproducibility.

We then expanded our study to include the Lactate-responsive bacterial biosensor using the same CHL-responsive genetic pathway employed in the Heme-responsive strain (Fig. 3i–l). Followed a similar experimental protocol to Heme-responsive strain co-culture (Fig. 3i and j): Either the IFFL circuit (Fig. 3b) or the direct regulation circuit (Fig. 3a) was combined with the Lactate-responsive strain (Fig. 3d) at a 1:1 ratio in volume, and added the AHL/Lactate inducer based on four distinct states: without any inducers ('00'), with Lactate alone ('01'), with AHL alone ('10'), and with both Lactate and AHL present ('11'). The experiments were conducted with AHL at a concentration of 2 μM and Lactate at 10 mM. This Lactate concentration approaches the range where the Lactate-biosensor reaches its maximum activity (Supplementary Fig. 15).

In the direct regulation co-culture experiments involving Lactate-responsive bacterial biosensors (Fig. 3i and k), the '00' state remains low, indicating minimal background activity without inducers. The '10' state, representing the presence of AHL only, shows a similar response compared to the '00' state in bioluminescence. However, a recurring issue is observed where the '11' state, intended to show a response from both AHL and another inducer, does not significantly differ from the '01' state. Conversely, in the IFFL co-culture (Fig. 3j and l), the '00' and '01' states show minimal bioluminescence throughout the observation period. The '10' conditions exhibit very little change from the baseline, indicating that neither Lactate nor AHL alone substantially increases bioluminescence in this IFFL co-culture. Similar to the result of Heme-responsive co-culture (Fig. 3h), in the IFFL co-culture scenario (Fig. 3j and l), the state '11' state displayed an enhanced response compared to '01', '10', and '00' states. IFFL co-culture further emphasizes its capability to control the temporal progression of different input signals. The OD_{600} signal for the Lactate-responsive strain co-culture is illustrated in Supplementary Fig. 16.

https://doi.org/10.1038/s41467-025-58996-9

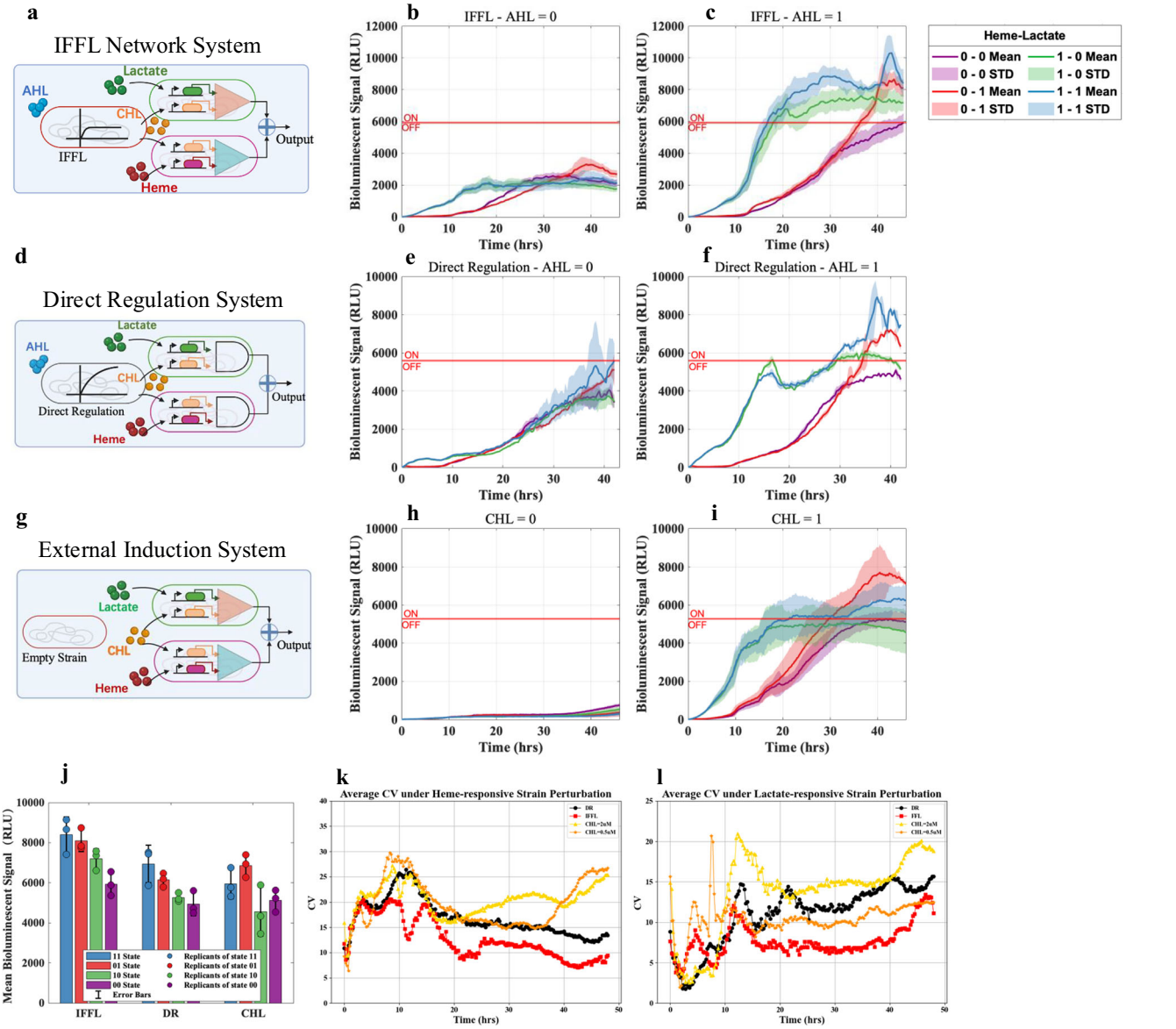

Fig. 4 | Microbial consortium-based biosensors. a-c Representations of the IFFL Network System in vitro. **a** Schematic gene circuit diagrams for IFFL Network System. **b**, **c** Dynamic response in the absence of AHL inducer (**b**) compared to its presence (**c**). **d**–**f** Representations of the Direct Regulation System. **d** Schematic gene circuit diagrams for the Direct Regulation System. Dynamic response in the absence of AHL inducer (**e**) compared to its presence (**f**). **g**–**i** System representations with externally added CHL (External Induction System). The empty strain containing only the antibiotic and plasmid copy number. **g** Schematic diagram of the gene circuit for the External Induction System. **h** Dynamic response in the absence of CHL inducer compared to (**i**) its presence. The threshold (red horizontal line) for the systems is based on the average curve from the three replicates. And the threshold is set as the maximum value observed among the following five states: the four states ("00," "01," "10," and "11") when AHL = 0, and the "00" state when AHL = 1. **j** Mean bioluminescent signals at their threshold level across states '11', '01', '10', and '00' for three systems: IFFL Network System (IFFL), Direct Regulation (DR), and External Induction System. Each state's mean value is shown in a bar chart, with individual replicates represented as small circles on each bar. The four states are represented in distinct colors: '11' (blue), '01' (red), '10' (green), and '00' (purple). Error bars indicate the standard deviations of the three replicates. **k**, **l** The coefficient of variation (CV) for the IFFL Network System (red square curve), Direct Regulation System (black dotted curve), and External Induction System (yellow triangle curve for CHL = 2 μM and orange stars curve for CHL = 0.5 μM) under perturbations from the Heme-responsive strain (**k**) or Lactate-responsive strain (**l**). Source data are provided as a Source Data file. Figure **a**, **d** and **g** created with BioRender.

Microbial consortium-based biosensors

We then developed three distinct consortia configurations to detect Heme and Lactate simultaneously. The first configuration utilized the IFFL strain to generate the CHL shared signal (IFFL Network System, Fig. 4a). The second configuration employed the direct regulation strain for CHL production (Direct Regulation System, Fig. 4d). The third configuration relied on supplying the CHL signal externally (External Induction System, Fig. 4g). The data normalized to bioluminescence/ OD_{600} (RLU/ OD_{600}) was displayed in Supplementary Fig. 17, and the OD_{600} is shown in Supplementary Figs. 18–20. Each colony's dynamic behavior for the corresponding system is shown in Supplementary Figs. 21–23. Inducers (AHL, Heme, and Lactate) were added simultaneously to the three systems in the beginning of the experiments. The dynamic responses of the IFFL Network System (Fig. 4b, c, Supplementary Fig. 24A, B), the Direct Regulation System (Fig. 4e, f, Supplementary Fig. 24C, D), and the External Induction System (Fig. 4h, i, Supplementary Fig. 24E, F) were measured for >40 h. A threshold level was established to classify the system's states into low

and high activity as follows: (1) low state, where there is no consortium activity, which may occur either due to the absence of biomarkers despite a high enable signal (CHL) or the absence of the enable signal even if the biomarker levels are high; and (2) high state, where there is high consortium activity. Accordingly, the threshold was set at the maximum value among five states, including the four states ("00", "01", "10", and "11") when AHL = 0 and the "00" state when AHL = 1. The '00' condition signifies that neither Heme nor Lactate is present, serving as the baseline state; '01' indicates the presence of Lactate alone; '10' represents the presence of Heme alone; and '11' denotes that both Heme and Lactate are added, allowing for the assessment of their combined effect on the system.

The dynamic responses of the three systems, measured under conditions of low (Fig. 4b, e, and h) and high (Fig. 4c, f, and i) inducer levels (AHL in the case of IFFL Network System and Direct Regulation System, and CHL in the case of External Induction System), illustrate the role of the shared signal as a enable mechanism. Based on the measured results, the thresholds for the IFFL Network and External Induction Systems were observed at AHL = 1, Heme=0, and Lactate=0 (Fig. 4c, i), while the threshold for the Direct Regulation System occurred at AHL = 0, Heme=1, and Lactate=1 (Fig. 4e). Accordingly, the consortia output is engineered to remain at low levels regardless of the activities of the Heme and Lactate-responsive strains when shared signal levels are low (Fig. 4b, e, and h). When AHL is high in the IFFL Network System and Direct Regulation System, or CHL is high in the External Induction System, the output of all three systems (Fig. 4c, f, and i) reflects the activity of the input strains, allowing the shared signal to modulate the Heme and Lactate activities by generating a common bioluminescent output signal. In the three configurations, the outputs from the Heme and Lactate-responsive strains are combined to trigger a single readout output, effectively evaluating the consortium's capability to integrate temporally distinct signals through analog summation ($Out_{Total}(t) = Out_{Heme}(t) + Out_{Lactate}(t)$) (Fig. 1b and Supplementary Fig. 25)[51,53]. This result also suggests the coexistence of the Heme-responsive and Lactate-responsive strains.

The IFFL Network System (Fig. 4c) response at AHL = 1 can differentiate among the four states ('00', '11', '01', and '10') particularly after 15 h. In contrast, the Direct Regulation System (Fig. 4f) response at AHL = 1 can only distinguish between the '00' and '10' states after 30 h. The External Induction System (Fig. 4i), however, fails to differentiate between the '00' and '10' states. When the data is normalized by computing the ratio of the measured signal to cell concentration, both the Direct Regulation and External Induction Systems (Supplementary Fig. 17) are able to distinguish between the '00' and '01' states after 10 h. This result aligns with our theoretical model (Eq. 19 in the section ' Mathematical Modelling for Signal Coupling in Microbial Consortia' in Methods). In addition, to evaluate the ability of the three systems to clearly distinguish the '00' state from its threshold level in Fig. 4c, f, and i, we conducted a statistical analysis to estimate the p-value (Fig. 4j), yielding $p = 0.049$ for the IFFL Network System, $p = 0.419$ for the Direct Regulation System and $p = 0.504$ for the External Induction System. Our calculation was based on comparing the mean bioluminescent signals at the end time point across the '11', '01', '10', and '00' states for three systems. For both the IFFL Network and Direct Regulation Systems (Fig. 4j), the '10' state exhibited the closest to that of the '00' state among the '10', '01', and '11' states, with the Direct Regulation system reaching this point at 43 h and the IFFL Network System at 46 h. For External Induction System, the '01' state exhibited the closest to that of the '00' state among the '10', '01', and '11' states. The p-value was determined by conducting an independent two-tailed t-test between the endpoints from the corresponding state and threshold curves in these three systems. We also calculated the fold-change rate in the bioluminescent signal over time by computing the derivative of the output ($dOut/dt$) (Supplementary Fig. 26). The signal derivative of the IFFL Network System shows minimal variation across the four logic states of Lactate and Heme when AHL = 0, with significant changes in the other states when AHL = 1 except for the '00' state. In contrast, the Direct Regulation System displayed high changes in the signal derivative for the '11' state, with values similar to those observed under both low and high AHL conditions (Supplementary Fig. 26). Although the External Induction System exhibited high variability in response to the absence and presence of CHL, it failed to demonstrate a significant change when Lactate was added under conditions of high CHL.

Finally, we tested the consortia's robustness by adding initial perturbations in the cell population of bacterial biosensor strains (Fig. 4k and l). Specifically, we manipulated the volumes of Heme-responsive strains or Lactate-responsive strains while maintaining constant volumes for the other two strains. The volume of the changing strain (Heme-responsive strains or Lactate-responsive strains) varied from 60 μL to 140 μL, whereas the volumes for the other biosensor strain and the shared signal consortium were maintained at 100 μL, consistent with previous experiments (Supplementary Figs. 27–34). To evaluate the robustness of the three systems, we calculated the Coefficient of Variation (CV) by computing the ratio between the standard deviation and the average signal ('Coefficient of Variation (CV)' in Supplementary Methods). The CV for the IFFL Network System is consistently lower than other systems during the time range of 16 to 42 h, highlighting the better robustness of the IFFL Network System. Under Heme-responsive strain perturbation, the CV values were 10.7% for the IFFL Network System, 15.2% for the Direct Regulation System, and 20.0% and 18.8% for the External Induction System with 2 μM and 0.5 μM CHL, respectively. Similarly, under Lactate-responsive strain perturbation, the CV values were 7.9% for the IFFL Network System, 12.8% for the Direct Regulation System, and 15.6% and 10.6% for the External Induction System with 2 μM and 0.5 μM CHL, respectively. These values represent the time-average CV across the different conditions observed once the signals begin to reach a steady state (>15 h). The IFFL Network System demonstrated a 46% improvement in robustness compared to the Direct Regulation System under Heme-responsive strain perturbation, and 90% and 77% improvements compared to the External Induction System with 2 μM and 0.5 μM CHL, respectively. Under Lactate-responsive strain perturbation, the IFFL Network System demonstrated a 72% improvement in robustness compared to the Direct Regulation System and 107% and 42% improvements compared to the External Induction System with 2 μM and 0.5 μM CHL, respectively (Supplementary Fig. 35). A similar conclusion regarding the robustness of the three systems against cell fluctuations can be observed from the results of the stochastic simulation (Supplementary Fig. 50). Our analytical modeling (Eq. (26) in section 'Mathematical Modelling for Signal Coupling in Microbial Consortia' in Methods) reveals that when strain fluctuations are small (<10%), the IFFL-based consortia exhibit enhanced robustness compared to its direct regulation-based counterpart.

Coupled consortia for feces diagnostic

We also tested our systems with mouse fecal samples to detect Heme and Lactate biomarkers. Heme and Lactate were chosen for their relevance in fecal diagnostics, where their presence may signal potential gastrointestinal health concerns. In this study, we used Lactate at 10 mM and Heme at 2 μM in the in vitro experiments (Fig. 5c, d, Supplementary Fig. 36). This Lactate concentration has strategically selected a lower threshold level as a marker for unhealthy conditions in pathological humans[57–59]. Notably, the summation relationship between these biomarkers underscores their individual significance in the diagnostic process - the presence of either biomarker is sufficient to trigger a response in the system. The procedure for fecal sample preparation is illustrated in Fig. 5a. For all experiments conducted within the fecal sample, we maintained a 1:1 volume ratio between the engineered bacteria consortium sample and the filtered fecal media sample, with the AHL and biomarkers being added before the filtering

https://doi.org/10.1038/s41467-025-58996-9

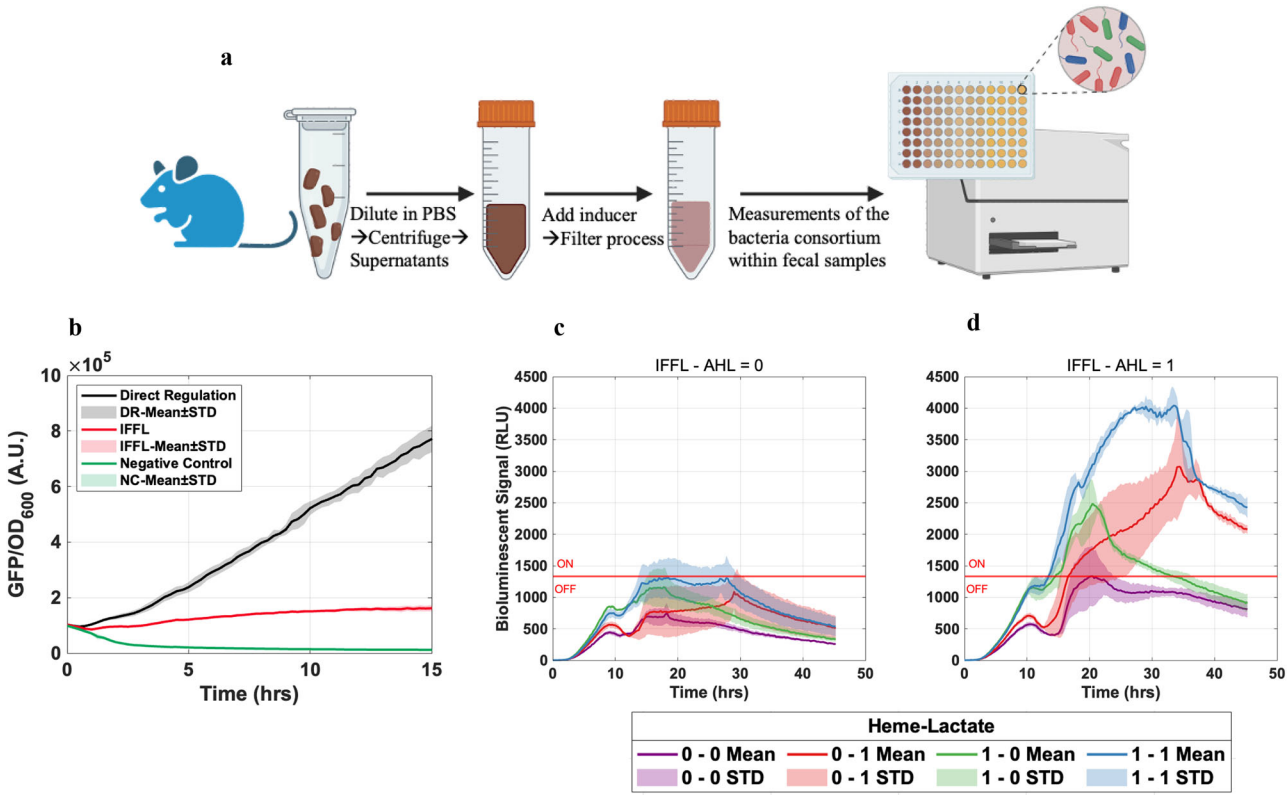

Fig. 5 | Coupled consortia for feces diagnostic. a Procedure for fecal sample experiments: (1) Collection of fecal samples from humanized mice. (2) Suspension of fecal samples in sterile PBS, followed by centrifugation to collect the supernatants. (3) Adding the inducers to the supernatants and subsequent filtration of the mixture. (4) Mixing of the bacterial co-culture with the filtered supernatants, with measurements taken using a microplate reader. **b** GFP/OD_{600} response dynamics of the IFFL network (IFFL, red curve), the direct regulation (DR, black curve), and the negative control circuit (NC, green curve) within fecal samples. **c**, **d** Dynamics response of the IFFL Network System in the absence (**c**) and presence (**d**) of AHL within the filtered fecal sample. Source data are provided as a Source Data file. Figure **a** created with BioRender.

process. The necessity of the filtering process is explained in Supplementary Fig. 37. In the unfiltered samples, the high and consistent background OD_{600} during the measurements masked the actual dynamics of bacterial growth. Thus, we recommend filtration when detecting small molecules in fecal samples. We followed a recently developed protocol allowing the measurement of green fluorescent signals from fecal samples[60].

First, we validated the consistency of the Direct Regulation and IFFL networks in filtered fecal samples (Fig. 5b), confirming alignment with the results observed in our in vitro experiments. The output signal of the direct regulation circuit (the same genetic circuit used in vitro experiments from Fig. 2b) increased continuously over time, failing to reach a saturation point within the 15-h timeframe (Fig. 5b, black curve). By contrast, the IFFL network from Fig. 2a displayed a relatively stable expression within the fecal sample throughout the measurement period (Fig. 5b, red curve). The output signal of the IFFL network is higher than that of the negative control (Fig. 5b, blue curve, engineered bacteria circuit containing only the antibiotic and plasmid copy number). Compared to in vitro experiments (Fig. 2d), the expression levels for both co-cultures are notably reduced. The OD_{600} signal is shown in Supplementary Fig. 38.

We examine our consortia in three steps. The first step included a Heme-responsive strain with the direct regulation or IFFL strains within the filtered fecal sample media (Supplementary Figs. 39–40). The second step included a Lactate-responsive strain with the direct regulation or IFFL strains within the filtered fecal sample media (Supplementary Figs. 41–42). In both steps, we observed a behavior similar to in vitro experiments. Finally, we tested the consortia, including the three strains (the same consortium design used in vitro experiments from Fig. 4a): IFFL, Heme, and Lactate-responsive strains with the absence and presence of AHL. Based on the corresponding states, inducers (AHL, Heme, and Lactate) were introduced at the beginning of the experiment. We then examined these coupled consortia over 40 h to detect and monitor the presence of Lactate and Heme in humanized fecal samples (Fig. 5c, d, Supplementary Fig. 36). In the presence of AHL (Fig. 5d), the '11' state initially reflects the behavior of the '10' state for the first 25 h. During this phase, the output signal reflects the Heme-responsive strain's reaction. Then, starting around the 30 h mark, the '11' state began to mirror the dynamics of the '01' condition, representing the Lactate-responsive strain's behavior. Therefore, the '11' signal is able to successfully reflect the multiple consortium-based input signals, aligning the dynamic of each individual input and providing a more robustness output in the fecal sample for diagnostic purposes (Supplementary Fig. 43). Additionally, we tested the consortia's robustness in response to minor perturbations in the populations of the individual bacterial biosensor strain (Supplementary Figs. 44). The IFFL Network System shows better robustness compared to the Direct Regulation System. In this experiment, the data is presented as the measured bioluminescence signal without normalization by cell concentration, reflecting strategies common in practical applications where measuring OD_{600} is often not feasible. The OD_{600} signal is shown in Supplementary Fig. 45. Additionally, we provide results (Supplementary Fig. 46) from inflamed acute colitis murine model fecal samples that were inherently bleeding demonstrating that our Heme sensor can detect inflammatory fecal samples. We used an acute colitis murine model induced by dextran sodium sulfate (DSS) (Methods). The bioluminescent response observed in the DSS-treated samples with CHL indicates the sensor's sensitivity to

pathological states, validating the sensor's application in biologically relevant scenarios of inflammation.

Discussion

In this study, we demonstrate that synthetic bacterial biosensors within consortia can be coupled through shared signaling molecules. Compared to systems where CHL is either externally supplied or internally produced by the direct regulation circuit, the IFFL network ensures consistently low-level CHL signaling, thereby effectively coupling the individual bacterial sensors in a consortium. Through computational simulations and experimental analysis, we have identified that systems under IFFL control exhibit enhanced robustness with respect to variations and perturbations in cell concentration. We also observe indications of coexistence between the Heme-responsive and Lactate-responsive strains (Fig. 4c and f). In the IFFL Network System configuration, the output of the synthetic consortia regulated by the IFFL exhibits reduced dependence on cell concentration within the consortium, which is advantageous in environments where maintaining a consistent cell concentration is challenging.

Our insights mark significant progress in developing large, synthetic multicellular systems. By harnessing this method to simultaneously initiate biosensors that detect multi-markers within fecal samples, we highlight its capacity to operate in resource-limited environments, demonstrating its potential for future medical applications and scaling up systems. Our approach is versatile and can be adapted to monitor various biomarkers in feces, as well as other healthcare environments such as urine and sweat. However, for each application, the detection window and time intervals would need to be adjusted accordingly.

Multi-marker cell-based biosensors with a single output and a single chamber simplify the biosensor system by reducing the complexities associated with multi-chamber biosensors and photodetector configurations. By contrast, biosensors equipped with multiple chambers tend to be expensive and highly power-consuming, thereby limiting their applicability in many biomedical and environmental contexts. For instance, an ingestible capsule has been recently developed for the in-situ detection of labile inflammatory biomarkers[61]. This system measures the activity of bioluminescent bacteria-based biosensors within two separate chambers. However, adding more chambers to measure additional biomarkers would result in an impractical increase in capsule size and hinder practical application. When this capsule requires the measurement of multiple biomarkers, the solution lies in designing multi-marker biosensors with a single output. Similarly, a remote detection system for buried landmines using bacterial biosensors has been developed[3]. If this system were to measure different types of explosive materials, the most viable approach involves designing multi-marker biosensors with a single output. Furthermore, in both of these examples, due to the challenge of real-time signal normalization with respect to biosensor cell concentration (OD_{600}), unlike our system, where the measured signal is much less dependent on biosensor cell concentration, our system is expected to provide more precise and reliable data.

Another potential application of our synthetic IFFL network is in gene expression studies. A stable output regulation facilitates accurate tracking of these temporal changes, ensuring a reflection of the true biological state. Similarly, in therapeutic-based living cells[62], stabilized transient responses can play a pivotal role in optimizing treatment outcomes. Consistent drug production, be it in the context of bacterial cancer therapies or engineered probiotics for treating inflammatory bowel disease (IBD)[63], is significantly important. The stable transient response of our network can be incorporated as a drug-release module within these therapeutic cells, guaranteeing a uniform drug dose over the entire treatment duration.

Our stabilization IFFL circuit can also be useful in metabolic engineering. It can enhance the production yield of targeted chemicals within synthetic bio-production pathways. These pathways frequently necessitate the removal of endogenous genes linked to cell growth and upkeep. However, this gene deletion ultimately leads to low growth rates[64], significantly impacting the eventual yield of the desired bio-product. Therefore, achieving a stable response through low-level expression of these endogenous genes could address this challenge.

Methods

Chemicals and biological samples

Sodium Lactate (L-lactate), hemin (ferric chloride heme or Heme), acyl-homoserine lactone 3OHC14:1-HSL (CHL), and acyl-homoserine lactone 3OC6HSL (AHL) were used as inducers (Sigma–Aldrich, Germany). A stock solution of Heme was prepared by dissolving hemin powder in 1 M NaOH (Sigma–Aldrich, Germany) to a concentration of 25 mM, diluting with double distilled water to a final concentration of 100 μM, and sterilizing with a 0.22 μm polyethersulfone (PES) filter. All the chemicals were of the highest analytical grade. The experiments were conducted with AHL at a concentration of 2 μM, Lactate at 10 mM, and Heme at 2 μM.

Ethics

All mouse work was in accordance with protocols approved by the local Technion, Israel, The Institutional Animal Care and Use Committee (IACUC) under approval numbers: IL-151-10-21 and IL-135-09-22.

Human donor feces were collected from a healthy male individual volunteer with informed consent, according to Rambam Health Care Campus (RAMBAM) medical center IRB approval NCT03167398.

Mice humanization

Four to five weeks-old Germ-Free (GF) C57BL/6 mice (males and females) from the Technion colony were used. Mice were housed and maintained in a GF care facility and were provided with food and water ad libitum; they were exposed to a 12:12 h light-dark cycle at room temperature. Human stool sample were frozen at −80 °C before processing. Humanized mice were generated by orally gavaging GF C57BL/6 mice with 200 μL of a fecal suspension prepared from a single healthy human donor, in which 1 gram of feces was suspended in 10 mL of sterile PBS (1:10 w/v)[65].

Acute DSS-induced colitis mouse model

For acute DSS-induced colitis in humanized mice, male and female mice were co-housed separately, and then treated with 3% (w/v) DSS in their drinking water for 8 days[66]. The control animals were administered distilled water. Fecal samples for analysis were collected on day 8, coinciding with the end of the treatment and the day of sacrifice. Daily assessments included monitoring body weight, stool consistency, and blood in the rectum or stool. Throughout the experiments, close attention was paid to monitor any distress responses exhibited by the mice: mice with a 20% decrease in body weight, immobility, or an extreme reaction to touch, were excluded from the experiments.

Feces suspension

Mice fecal samples (30–50 mg) were flash-freezed in liquid nitrogen and then stored at −80 °C[67], and suspended in sterile PBS in 1 ml/100 mg feces, centrifuged at 4500 x g for 15 min, and supernatants were collected as the nonfiltered sample. If needed, filtered using the Medical Millex-VV Syringe Filter Unit, 0.22 μm, PVDF membrane or Corning sterile 96-well filter plate with polystyrene insert, 0.2 μm, PVDF hydrophilic membrane (Corning Incorporated, Kennebunk, ME, USA). When filtered with a plate, the samples were separated for 200 μL in each well, centrifuged at 4500 x g for 15 min, and collected. All the steps were done on ice.

Bacterial strains

The *Escherichia coli* (*E. coli*) 10β strain from New England Biolabs (Beverly, MA) was used to construct all plasmids, and in the kinetics experiments (genotype: araD139 D (ara-leu) 7697 fhuA lacX74 galK (W80 D (lacZ) M15) mcrA galU recA1 endA1 nupG rpsL (StrR) D (mrr-hsdRMS-mcrBC)). Chemically and electroporation-competent *E. coli* cells were prepared using standard protocols[68,69].

Plasmid construction

All the plasmids in this work were constructed using basic molecular cloning techniques[69] or Gibson Assembly[70]. Detailed plasmid maps, combinations, and genetic parts are provided in the Supplementary Information. The plasmids were modified by restriction digests, performed using New England Biolabs (Beverly, MA) restriction endonucleases and FastDigest restriction enzymes (ThermoFisher Scientific Inc., USA). For ligation, T4 DNA ligase and Taq polymerase were used (New England Biolabs, Beverly, MA). PCR was performed with a Bio-Rad S1000 thermal cycler with dual 48/48 fast reaction modules. Oligonucleotides were synthesized by Integrated DNA Technologies (Coralville, IA)—the manipulation of different parts (i.e., replacing promoters or genes) using the same restriction sites. Gibson assemblies were carried out using New England Biolabs (Beverly, MA) NEBuilder HiFi DNA assembly cloning kit. Plasmids were transformed into *E. coli* using a standard heat shock protocol[69] or a MicroPulser electroporator[68]. Colony PCR screening was carried out using forward and reverse primer pairs. Positive clones were sequence-verified. According to the manufacturer's instructions, plasmids were isolated with Promega Wizard Plus SV Minipreps DNA Purification Systems (Promega Corporation, Madison, WI, USA). The Macrogen Sequencing Service performed DNA sequencing (Macrogen Europe, The Netherlands).

Bacterial culture

Escherichia coli strains were stored as glycerol stocks at −80 °C and then grown at 37 °C in a Shel Laboratories SSI5 shaking incubator at 250 rpm in 5 mL of Lysogeny broth (LB-Miller) medium (Fisher), supplemented with carbenicillin (50 μg/mL), kanamycin (30 μg/mL), or chloramphenicol (34 μg/mL). Overnight cultures were diluted 100-fold into 5 mL of fresh LB medium with antibiotics and regrown with shaking at 37 °C and 250 rpm for 0.5 h ($OD_{600} \approx 0.1$).

For the M9 + 0.4% glucose media experiment (Supplementary Fig. 10), the cells were overnight cultured in LB and were diluted 1:50 into fresh M9 + 0.4% glucose medium [1× M9 Salts (Sigma–Aldrich, M6030), 2 mM $MgSO_4$, 100 μM $CaCl_2$, 0.4% glucose, 0.1% casamino acids, 50 mg/l thiamine]. The cultures were incubated for 1 hr for the M9 + 0.4% glucose media experiment or 30 min for other experiments at 37 °C with 250 rpm and then measured with a plate reader. GFP signals were read at 15 min intervals using a Synergy H1 monochromator-based multimode microplate reader with continuous shaking at 500 rpm and a constant temperature of 37 °C. GFP fluorescence was quantified by excitation at a wavelength of 485 nm and emission at a wavelength of 516 nm. Unless otherwise stated, all experiments were repeated with three replicants. GFP values were measured in arbitrary relative fluorescence units (RFUs), and the normalized signals were calculated by dividing these values by the OD_{600}.

Feces preparation for experiments

Centrifuged feces supernatants were collected and mixed with various concentrations of Heme/Lactate/AHL/CHL or their combinations and filtered as the states needed. When non-filtered, only top-layer supernatant was collected and supplemented with inducers. Either filtered or non-filtered mice feces supernatants were prepared and complemented with carbenicillin (50 μg/mL), kanamycin (30 μg/mL), or chloramphenicol (34 μg/mL).

Microplate reader kinetics experiments

Culture aliquots (150 μL) were transferred into wells of 96-well plates, mixed with various concentrations of Heme/Lactate/AHL/CHL or their combinations diluted in 150 μL of LB/sterile PBS, or for fecal supernatants experiments. The inducers were included in the sample. Luminescence and green fluorescent protein (GFP) signals were read at 15- or 20 min intervals using a Synergy H1 monochromator-based multimode microplate reader with shaking at 500 rpm and a constant temperature of 37 °C for GFP experiments and 23 °C for luminescence. The luminescence signal was measured at 490 nm. GFP fluorescence was quantified by excitation at a wavelength of 485 nm and emission at a wavelength of 516 nm. Luminescence and GFP values were measured in arbitrary relative fluorescence units (RFU) and luminescence units (RLUs), and the normalized signals were calculated by dividing these values by the optical density (OD_{600}) of the culture measured at 600 nm. Unless otherwise stated, experiments were conducted in triplicate.

Experiments using FACS

Flow cytometry analyzer voltages were adjusted using CyExpert 2.2 software to ensure that both maximum and minimum expression levels could be accurately measured under the same voltage settings, which were consistently maintained throughout all experiments, including repeated runs. GFP was excited with a 488 nm laser, and each FACS run acquired 10,000 events with an abort rate below 2%. Fluorescence, along with forward and side scatter measurements, was recorded using CyExpert 2.2 software. The geometric median of the gated fluorescence distributions was calculated using MATLAB, and fluorescence values, expressed in arbitrary units (arb. units), were based on the geometric medians from three independent experiments. Cells were first gated based on forward scatter (FSC-A) and side scatter (SSC-A) to identify the major viable population, typically comprising over 90% of the total cell population. Fluorescence intensity was then measured for the gated population to assess the relevant markers. Flow cytometry data from one representative experiment is provided in Supplementary Fig. 8 and Supplementary Table 1.

Analog signal control in biosensor consortia

Under certain conditions, where the concentration of the total shared signal distributed across the entire consortia ($S_T = \sum_{i=1}^{M} S_i$, where S_i is the shared signal for each consortium) is lower than that of the total cell concentration ($S_T \ll \sum_{i=1}^{M} N_i$), can facilitate a coupling among the diverse cells. This, in turn, reduces the influence of cell concentration within each consortium on the overall output signal $Out \propto \frac{\sum_{i=1}^{M} N_i f_i}{\sum_{i=1}^{M} N_i}$ (Fig. 1a and Supplementary Fig. 1). Furthermore, if the shared signal is inducible, it can serve as an enable signal for externally regulating the system output (Fig. 1b). This control signal functions as a conditional gate: when the signal is at a high level, it permits the transmission of the biosensor's response, effectively "enabling" the system's output ($S_T = High, Out = f,\ t > t_0$). Conversely, it prevents signal transmission when the control signal is in a low level state ($S_T = Low, Out = 0, t < t_0$). The realization of a circuit incorporating an enabled control signal is comparatively complicated in the analog domain compared to the digital domain. In digital circuits, enabling can be accomplished using an AND logic gate. In analog circuits, e.g., biosensors, the implementation involves a circuit that computes the minimum between the activity of the enable signal and the analog response of the input signal; $MIN\{g(Enable), f(In)\}$ (i.e., $MIN\{Low, f\} = 0$, *and* $MIN\{High, f\} = f$) (Supplementary Fig. 1). On one hand, the ON level must be lower than the total cell concentration to couple the cells effectively (Methods). On the other hand, the ON level of the enable signal should exceed the activity of each biosensor to ensure proper computation of the minimum operation. Thus, programming the

correct ON level of the shared signal is challenging. Enabling is also considered a foundational step toward achieving member coordination within consortia. Without proper coordination, temporal misalignments between cellular activities may give rise to significant consequences, encompassing undesired cellular responses[14,15].

Conceptual and mathematical examination of the IFFL network dynamics

In the diagram of the IFFL network (Fig. 2a), the molecule x activates both molecules y and z with rates α_1 and ρ, respectively. Furthermore, in this normalized equation, molecule y inhibits molecule z with a dissociation constant of k and a Hill coefficient of n. The degradation rates of z equals γ_2, of y equals γ_1. The Ordinary Differential Equation (ODE) for molecule concentration of z and y are given by:

$$\dot{z} = \rho \frac{x}{1 + \left(\frac{y}{k}\right)^n} - \gamma_2 \cdot z \tag{1}$$

$$\dot{y} = \alpha_1 \cdot x - \gamma_1 \cdot y \tag{2}$$

For the direct regulation (Fig. 2b), the production rate of z is α_0 and the degradation rates of z equals γ_0. The ODE in this case for molecule z is represented as:

$$\dot{z} = \alpha_0 \cdot x - \gamma_0 \cdot z \tag{3}$$

We begin by illustrating this stability response's conceptual underlying in the network's dynamic performance. We use kn to illustrate the comparation between the repression pathway to the activation pathway, $k_n = \frac{k \cdot \gamma_1 \cdot \rho}{\alpha_1 \cdot \gamma_2}$. Our mathematical analysis of the IFFL network (Eqs. (1) and (2)) demonstrates three different behaviors using a step function input for x:

1. Fold change detection: Within this interval, the initial rise in output (illustrated by the green curve $k_n = 0.01$) stems from the direct activation of z by x (through activation pathway A in Fig. 2a). This is followed by a decrease brought about by y's time-delayed repression. As repression initiates with an increase in y levels, a strong decrease ensues, resulting in a pulse-like pattern of behavior. When $k_n \ll 1$, the robust repression enables the system to revert to its baseline state following the initial stimulus. This behavior is known as perfect adaption.
2. Enduring stability: In this interval, a stable output arises from the equilibrium between activation and repression. As shown in Fig. 2c, where $k_n = 1.5$ (red curve) and $k_n = 0.5$ (blue curve), the IFFL network accelerates the response speed compared to a directly regulated network, leading to an earlier reach of a steady state. In the IFFL, while maintaining the network parameters constant, we varied the parameter k_n to explore its impact on network dynamics.
3. For a large value of $k_n > 1$, the activation will be the dominant process, resulting in a behavior similar to that of the directly regulated network.

As conclusion: a trade-off arises in the IFFL network dynamics; strong repression typically results in an accelerated, pulse-like response, while a stable output is usually achieved with weaker repression.

We selected the IFFL for this work because of its ability to maintain stability ($k_n > 1$) over extended periods.

Mathematical modelling for signal coupling in microbial consortia

To enhance coupling within the consortia system, we formulated a strategy employing a common signaling molecule, S, among various bacterial strains. This study assumes that S signal is coupling only two engineered bacterial consortia, each designed for a distinct biosensor function. These biosensors are customized to detect specific input signals (I_{n1} and I_{n2}) while also being responsive to the shared signaling molecule S. Our mathematical dynamic model utilizes cooperative interactions across the consortium and is given by:

$$S + E_1 \underset{K_{m1}}{\leftrightarrow} SE_1 \tag{4}$$

$$S + E_2 \underset{K_{m2}}{\leftrightarrow} SE_2 \tag{5}$$

$$P_1 + SE_1 \underset{K_1}{\leftrightarrow} Z_1 \tag{6}$$

$$P_2 + SE_2 \underset{K_2}{\leftrightarrow} Z_2 \tag{7}$$

Here, E_i denotes the concentration of a transcription factor that can interact with S across both biosensor types, while SE_i represents the fraction of the transcription factor bound to S. Furthermore, P_i (where $i = 1,2$) indicates the production concentration triggered by I_{n1} and I_{n2}, respectively. With K_{mi} and K_i as the dissociation constants for the respective reactions, the result is the production of Z_i (Z_1 and Z_2) molecules (Supplementary Fig. 47). At the steady-state, we can write:

$$SE_i = \frac{S \cdot E_i}{K_{mi}} \tag{8}$$

The total transcription factor level of each respective bacterial strain reveals:

$$E_{Ti} = E_i + SE_i \tag{9}$$

Here, we assumed that the total level of the transcription factor E_{Ti} is uniformly distributed across the same strain. The total level of the shared signal across the system is described by:

$$S_T = S + N_1 \cdot SE_1 + N_2 \cdot SE_2 \tag{10}$$

with N_1 and N_2 describe the bacterial population of each respective strain.

Assuming $K_{m1} = K_{m2}$ and $E_{T1} = E_{T2}$, the system dynamics can be simplified as:

$$\begin{cases} E_T &= E + SE \\ S_T &= S + (N_1 + N_2) \cdot SE \end{cases} \tag{11}$$

Combining these equations yields an expression for SE:

$$SE^2 - SE\left(E_T + \frac{S_T}{N_1 + N_2} + \frac{K_m}{N_1 + N_2}\right) + \frac{S_T}{N_1 + N_2} \cdot E_T = 0 \tag{12}$$

The solution is:

$$SE = \frac{E_T + \frac{S_T}{N_1+N_2} + \frac{K_m}{N_1+N_2} - \sqrt{\left(E_T + \frac{S_T}{N_1+N_2} + \frac{K_m}{N_1+N_2}\right)^2 - 4\frac{S_T}{N_1+N_2} \cdot E_T}}{2} \tag{13}$$

We can approximate this equation as:

$$SE = E_T \cdot \frac{S_T}{E_T \cdot (N_1 + N_2) + S_T + K_m} \tag{14}$$

Considering the dynamics described by Eqs. (6) and (7), P_1 and P_2 are functions of I_{n1} and I_{n2}; therefore $P_i = f_i(I_{ni})$. At the steady state, the output Z_i is given by the solution of the equation $Z_i = \frac{SE \cdot P_i}{K_i}$. Thus, the output Z can be described as:

$$Z = SE \cdot \left(\frac{N_1 \cdot f_1(I_{n1})}{K_1} + \frac{N_2 \cdot f_2(I_{n2})}{K_2} \right) \tag{15}$$

Using the above approximation, the total signal Z becomes:

$$Z = E_T \cdot \frac{S_T}{E_T \cdot (N_1 + N_2) + S_T + K_m} \cdot \left(\frac{N_1 \cdot f_1(I_{n1})}{K_1} + \frac{N_2 \cdot f_2(I_{n2})}{K_2} \right) \tag{16}$$

This expression suggests that the output signal is coupled by the shared signaling molecules S_T; the interplay between N_1 and N_2 is smoothed by their combined effect $(N_1 + N_2)$. The shared signal introduces an extra constraint on the system, consequently limiting its degree of freedom. Importantly, the signals $f_1(I_{n1})$ and $f_2(I_{n2})$ should be similar; otherwise, signal Z will be dominated by one of them.

On the other hand, for independent biosensors devoid of shared signaling, the output Z_{ind} is given by:

$$Z_{ind} = N_1 \cdot f_1(I_{n1}) + N_2 \cdot f_2(I_{n2}) \tag{17}$$

In the Z_{ind} expression, the total signal is influenced by N_1 and N_2 individually. Variations in one population directly impact the total output signal.

For system analysis in Eq. (16), we considered various conditions, including both high and low levels of shared signal S_T. Starting with high levels of S_T: $S_T + K_m \gg E_T \cdot (N_1 + N_2)$, the total signal shown in Eq. (16) is approximated by:

$$Z = E_T \cdot \frac{S_T}{S_T + K_m} \cdot \left(\frac{N_1 \cdot f_1(I_{n1})}{K_1} + \frac{N_2 \cdot f_2(I_{n2})}{K_2} \right) \tag{18}$$

The total output signal depends on the two strains of consortium separately, which is similar to the expression of the Z_{ind} in Eq. (17). In both scenarios, the output isn't adjusted by the bacterial population counts N_1 and N_2. However, for precise values of $f_1(I_{n1})$ and $f_2(I_{n2})$ and subsequent estimation of I_{n1} and I_{n2}, normalization by $N_1 + N_2$ is needed.

On contrast, for small S_T, meaning $S_T + K_m \ll E_T \cdot (N_1 + N_2)$ in Eq. (16) is approximated to:

$$Z = \frac{S_T}{(N_1 + N_2)} \cdot \left(\frac{N_1 \cdot f_1(I_{n1})}{K_1} + \frac{N_2 \cdot f_2(I_{n2})}{K_2} \right) \tag{19}$$

The output signal is already normalized by the total cell number $N_1 + N_2$. Consequently, there is no necessity to divide the measured signals by the total cell concentration when calculating the correct signals. The output normalization is simplified because the shared signal introduces an additional constraint, thereby confining the system with S_T.

Equation (19) also suggests that the system's output is more robust against fluctuations in bacterial population ratios. To further investigate this robustness and understand the potential effects of individual consortium variations, we postulated exponential growth for both bacterial strains, introducing a small difference in the growth rate specifically for the strain N_2.

$$N_1 = N_0 e^{\mu \cdot t} \tag{20}$$

$$N_2 = N_0 e^{(\mu + \Delta\mu) \cdot t} = N_1 e^{\Delta\mu \cdot t} \tag{21}$$

In case that $\Delta\mu \cdot t \ll 1$, we can approximate:

$$N_2 = N_1 \cdot (1 + \Delta\mu \cdot t) \tag{22}$$

For the output, Z_{ind} is given by:

$$Z_{ind} = N_1 \cdot (f_1(I_{n1}) + f_2(I_{n2})) + N_1 \cdot \Delta\mu \cdot t \cdot f_2(I_{n2}) \tag{23}$$

When S_T is large, and assuming that $K_1 = K_2 = K$. The Eq. (18) can be approximated as:

$$Z = \frac{E_T}{K} \cdot \frac{S_T}{S_T + K_m} \cdot N_1 \cdot (f_1(I_{n1}) + f_2(I_{n2}) + f_2(I_{n2}) \cdot \Delta\mu \cdot t) \tag{24}$$

The output Z depends on N_1 and the error term $f_2(I_{n2}) \cdot \Delta\mu \cdot t$. However, if the S_T is small, the Eq. (19) is approximated as:

$$Z = \frac{S_T}{2 \cdot \left(1 + \frac{\Delta\mu}{2} \cdot t\right)} \cdot \left(\frac{f_1(I_{n1})}{K_1} + \frac{f_2(I_{n2})}{K_2} + \frac{f_2(I_{n2})}{K_2} \cdot \Delta\mu \cdot t \right) \tag{25}$$

For $\frac{\Delta\mu}{2} \cdot t \ll 1$, we can approximate the term $\frac{1}{1 + \frac{\Delta\mu}{2} t} \approx 1 - \frac{\Delta\mu}{2} \cdot t$. Substituting the latter term into Eq. (25) and assuming $K_1 = K_2 = K$, we obtain:

$$Z = \frac{S_T}{2 \cdot K} \cdot \left(f_1(I_{n1}) + f_2(I_{n2}) + \frac{\Delta\mu}{2} \cdot t \cdot (f_2(I_{n2}) - f_1(I_{n1})) \right) \tag{26}$$

The output solution is independent of the concentration of strain population N_1 or N_2. Moreover, the error is much smaller than the error in the Eq. (24).

The results indicate that outputs for systems with lower S_T values are independent of individual strain concentrations, thereby offering a more robustness and normalized output compared to systems with larger S_T. Therefore, shared signal presents a method for coupled responses within a consortia, leading to outputs with greater precision and reduced calibration needs when utilized in devices.

We then performed simulations for consortia dynamics, including two biosensors. Specifically, we investigated the condition with and without a shared signal. The population dynamics and behavior of the input signals are detailed in Supplementary Figs. 48 and 49. Notably, Supplementary Fig. 50 demonstrates that when a shared signal couples the consortium, the final output, represented by the aggregation (sum) of the two biosensors, exhibits reduced sensitivity to fluctuations in cell population. Additionally, we evaluated the output signal using Eq. (16) for different S_T levels. There's a distinct reduction in noise, shown in Supplementary Fig. 51, when $S_T + K_m \ll E_T \cdot (N_1 + N_2)$ compared to the conditions with higher levels of S_T, where $S_T + K_m \gg E_T \cdot (N_1 + N_2)$.

Reporting summary

Further information on research design is available in the Nature Portfolio Reporting Summary linked to this article.

Data availability

All data used in this study is available in GitHub (https://github.com/LSB2/2025-Engineering-Coupled-Consortia-Based-Biosensors-for-Diagnostic.git) All relevant data are also available from the authors upon request. The raw data generated in this study are provided in the Supplementary Informationand Source Data file. Source data are provided with this paper.

Code availability

Computer code is available from GitHub under https://github.com/LSB2/2025-Engineering-Coupled-Consortia-Based-Biosensors-for-Diagnostic.git.

References

1. Calero, P. et al. A fluoride-responsive genetic circuit enables in vivo biofluorination in engineered Pseudomonas putida. *Nat. Commun.* **11**, 5045 (2020).
2. Chen, L. et al. Direct stimulation of de novo nucleotide synthesis by O-GlcNAcylation. *Nat. Chem. Biol.* **20**, 19–29 (2024).
3. Belkin, S. et al. Remote detection of buried landmines using a bacterial sensor. *Nat. Biotechnol.* **35**, 308–310 (2017).
4. Alnahhas R. N. et al. Majority sensing in synthetic microbial consortia. *Nat. Commun.* **11**, 3659 (2020)
5. Rapp, K. M., Jenkins, J. P. & Betenbaugh, M. J. Partners for life: building microbial consortia for the future. *Curr. Opin. Biotechnol.* **66**, 292–300 (2020).
6. Duncker K. E., Holmes Z. A. & You L. Engineered microbial consortia: strategies and applications. *Microb. Cell Fact.* **20**, 211 (2021)
7. Qian, Y., Huang, H.-H., Jiménez, J. I. & Del Vecchio, D. Resource competition shapes the response of genetic circuits. *ACS Synth. Biol.* **6**, 1263–1272 (2017).
8. Zhang R. et al. Winner-takes-all resource competition redirects cascading cell fate transitions. *Nat. Commun.* **12**, 853 (2021)
9. Ravikumar S., Baylon M. G., Park S. J. & Choi J. Engineered microbial biosensors based on bacterial two-component systems as synthetic biotechnology platforms in bioremediation and biorefinery. **14**, *62* (2017)
10. Müller, I. E. et al. Gene networks that compensate for crosstalk with crosstalk. *Nat. Commun.* **10**, 4028 (2019).
11. Kong, W., Meldgin, D. R., Collins, J. J. & Lu, T. Designing microbial consortia with defined social interactions. *Nat. Chem. Biol.* **14**, 821–829 (2018).
12. Tsoi R., Dai Z. & You L. Emerging strategies for engineering microbial communities. *Elsevier Inc.* **37**, 107372 (2019).
13. Chien, T. et al. Enhancing the tropism of bacteria via genetically programmed biosensors. *Nat Biomed. Eng.* **6**, 94–104 (2022).
14. Fontanarrosa, P. et al. Genetic circuit dynamics: hazard and glitch analysis. *ACS Synth. Biol.* **9**, 2324–2338 (2020).
15. Moon, T. S., Lou, C., Tamsir, A., Stanton, B. C. & Voigt, C. A. Genetic programs constructed from layered logic gates in single cells. *Nature* **491**, 249–253 (2012).
16. Cookson N. A. et al. Queueing up for enzymatic processing: Correlated signaling through coupled degradation. *Mol. Syst. Biol.* **7**, 561 (2011)
17. Liao, M. J., Din, M. O., Tsimring, L. & Hasty, J. Rock-paper-scissors: engineered population dynamics increase genetic stability. *Science* **365**, 1045–1049 (2019).
18. Liao, M. J., Miano, A., Nguyen, C. B., Chao, L. & Hasty, J. Survival of the weakest in non-transitive asymmetric interactions among strains of E. coli. *Nat. Commun.* **11**, 6055 (2020).
19. Miano, A., Liao, M. J. & Hasty, J. Inducible cell-to-cell signaling for tunable dynamics in microbial communities. *Nat. Commun.* **11**, 1193 (2020).
20. Brenner K., You L. & Arnold F. H. Engineering microbial consortia: a new frontier in synthetic. *Trends Biol.* **26**, 483–489 (2008).
21. Chen, Y., Kim, J. K., Hirning, A. J., Josić, K. & Bennett, M. R. Emergent genetic oscillations in a synthetic microbial consortium. *Science* **349**, 986–989 (2015).
22. Fiore, G. et al. In-silico analysis and implementation of a multicellular feedback control strategy in a synthetic bacterial consortium. *ACS Synth. Biol.* **6**, 507–517 (2017).
23. Liu, Y. X., Liu, S. B., Li, Y. M., Ye, Q. & Lai, X. Q. Design and implementation of a compact frequency synchronisation control circuit using enable input for DC-DC converter. *IET Power Electron.* **5**, 1827–1833 (2012).
24. Barone, F. et al. Design and evaluation of an incoherent feed-forward loop for an arsenic biosensor based on standard iGEM parts. *Synth. Biol.* **2**, ysx006 (2017).
25. Parkin J. M. & Murray R. M. Long-distance communication in synthetic bacterial consortia through active signal propagation. *bioRxiv* https://doi.org/10.1101/321307 (2018)
26. Parkin J. M., Hsiao V. & Murray R. M. Engineering pulsatile communication in bacterial consortia. *bioRxiv* https://doi.org/10.1101/111906.(2017)
27. Zong, D. M. et al. Tunable dynamics in a multistrain transcriptional pulse generator. *ACS Synth. Biol.* **12**, 3531–3543 (2023).
28. Alon, U. Network motifs: theory and experimental approaches. *Nat. Rev. Genet.* **8**, 450–461 (2007).
29. Yu F. et al. Biosynthesis, acquisition, regulation, and upcycling of heme: recent advances. *Crit. Rev. Biotechnol.* **44**, 1422–1438 (2024)
30. Voltarelli V. A., Alves de Souza R. W., Miyauchi K., Hauser C. J. & Otterbein L. E. Heme: the lord of the iron ring. *Antioxidants (Basel).* **12**, 1074 (2023)
31. Adegboyega David, T. R. Lower GI bleeding: an update on incidences and causes. *Clin. Colon. Rectal. Surg.* **33**, 28–34 (2020).
32. Hove, H. & Mortensen, P. B. Influence of intestinal inflammation (IBD) and small and large bowel length on fecal short-chain fatty acids and lactate. *Dig. Dis. Sci.* **40**, 1372–1380 (1995).
33. Manosalva, C. et al. Role of lactate in inflammatory processes: friend or foe. *Front Immunol.* **12**, 808799 (2022).
34. Kraut, J. A. & Madias, N. E. Lactic Acidosis. *N. Eng. J. Med.* **371**, 2309–2319 (2014).
35. Graboń, W. et al. Lactate formation in primary and metastatic colon cancer cells at hypoxia and normoxia. *Cell Biochem. Funct.* **34**, 483–490 (2016).
36. Basu, S. et al. Spatiotemporal control of gene expression with pulse-generating networks. *Proc. Natl Acad. Sci. USA* **101**, 6355–6360 (2004).
37. Segall-Shapiro, T. H., Sontag, E. D. & Voigt, C. A. Engineered promoters enable constant gene expression at any copy number in bacteria. *Nat. Biotechnol.* **36**, 352–358 (2018).
38. Kaplan, S., Bren, A., Dekel, E. & Alon, U. The incoherent feed-forward loop can generate non-monotonic input functions for genes. *Mol. Syst. Biol.* **4**, 203 (2008).
39. Greber, D. & Fussenegger, M. An engineered mammalian band-pass network. *Nucleic Acids Res.* **38**, e174 (2010).
40. Mangan, S., Itzkovitz, S., Zaslaver, A. & Alon, U. The incoherent feed-forward loop accelerates the response-time of the gal system of Escherichia coli. *J. Mol. Biol.* **356**, 1073–1081 (2006).
41. Alon U. *An Introduction to Systems Biology: Design Principles of Biological Circuits* 1st ed, Vol.320 (Chapman and Hall/CRC, 2019)
42. Kim, J. K. et al. Long-range temporal coordination of gene expression in synthetic microbial consortia. *Nat. Chem. Biol.* **15**, 1102–1109 (2019).
43. Goentoro, L., Shoval, O., Kirschner, M. W. & Alon, U. The incoherent feedforward loop can provide fold-change detection in gene regulation. *Mol. Cell* **36**, 894–899 (2009).
44. Litovco, P., Barger, N., Li, X. & Daniel, R. Topologies of synthetic gene circuit for optimal fold change activation. *Nucleic Acids Res.* **49**, 5393–5406 (2021).
45. Rizik, L., Danial, L., Habib, M., Weiss, R. & Daniel, R. Synthetic neuromorphic computing in living cells. *Nat. Commun.* **13**, 5602 (2022).
46. He, J., Zhang, X., Qian, Y., Wang, Q. & Bai, Y. An engineered quorum-sensing-based whole-cell biosensor for active degradation of organophosphates. *Biosens. Bioelectron.* **206**, 114085 (2022).
47. Shis, D. L. & Bennett, M. R. Synthetic biology: the many facets of T7 RNA polymerase. *Mol. Syst. Biol.* **10**, 745 (2014).
48. Bernhards, R. C., Jing, X., Vogelaar, N. J., Robinson, H. & Schubot, F. D. Structural evidence suggests that antiactivator ExsD from Pseudomonas aeruginosa is a DNA binding protein. *Protein Sci.* **18**, 503–513 (2009).
49. Shopera, T. et al. Robust, tunable genetic memory from protein sequestration combined with positive feedback. *Nucleic Acids Res.* **43**, 9086–9094 (2015).

50. Dasgupta, N., Lykken, G. L., Wolfgang, M. C. & Yahr, T. L. A novel anti-anti-activator mechanism regulates expression of the Pseudomonas aeruginosa type III secretion system. *Mol. Microbiol.* **53**, 297–308 (2004).
51. Winson, M. K. et al. Engineering the luxCDABE genes from Photorhabdus luminescens to provide a bioluminescent reporter for constitutive and promoter probe plasmids and mini-Tn 5 constructs. *FEMS Microbiol. Lett.* **163**, 193–202 (1998).
52. Barger, N., Litovco, P., Li, X., Habib, M. & Daniel, R. Synthetic metabolic computation in a bioluminescence-sensing system. *Nucleic Acids Res.* **47**, 10464–10474 (2019).
53. Anzai, T. et al. Expanded roles of lactate-sensing LldR in transcription regulation of the Escherichia coli K-12 genome: lactate utilisation and acid resistance. *Microb. Genom.* **9**, mgen001015 (2023).
54. Barger, N., Oren, I., Li, X., Habib, M. & Daniel, R. A Whole-cell bacterial biosensor for blood markers detection in urine. *ACS Synth. Biol.* **10**, 1132–1142 (2021).
55. Nobles, C. L., Clark, J. R., Green, S. I. & Maresso, A. W. A dual component heme biosensor that integrates heme transport and synthesis in bacteria. *J. Microbiol. Methods* **118**, 7–17 (2015).
56. Lechardeur, D. et al. Discovery of intracellular heme-binding protein HrtR, which controls heme efflux by the conserved HrtB-HrtA transporter in Lactococcus lactis. *J. Biol. Chem.* **287**, 4752–4758 (2012).
57. Li X. et al. Lactate metabolism in human health and disease. *Springer Nat.* **7**, 305 (2022)
58. Goedert, J. J. et al. Fecal metabolomics: assay performance and association with colorectal cancer. *Carcinogenesis* **35**, 2089–2096 (2014).
59. Kaalby, L. et al. Faecal haemoglobin concentrations are associated with all-cause mortality and cause of death in colorectal cancer screening. *BMC Med.* **21**, 29 (2023).
60. Zou, Z.-P., Yang, Y., Wang, J., Zhou, Y. & Ye, B.-C. Coupling split-lux cassette with a toggle switch in bacteria for ultrasensitive blood markers detection in feces and urine. *Biosens. Bioelectron.* **214**, 114520 (2022).
61. Inda M. E. et al. Ingestible capsule for detecting labile inflammatory biomarkers in situ. *bioRxiv* https://doi.org/10.1101/2022.02.16.480562 (2022).
62. Gurbatri, C. R. et al. Engineered probiotics for local tumor delivery of checkpoint blockade nanobodies. *Sci. Transl. Med.* **12**, eaax0876 (2020).
63. Pesce, M. et al. Next-generation probiotics for inflammatory bowel disease. *Int. J. Mol. Sci.* **23**, 5466 (2022). no. 10May.
64. Pitera, D. J., Paddon, C. J., Newman, J. D. & Keasling, J. D. Balancing a heterologous mevalonate pathway for improved isoprenoid production in Escherichia coli. *Metab. Eng.* **9**, 193–207 (2007).
65. Park, J. C. & Im, S.-H. Of men in mice: the development and application of a humanized gnotobiotic mouse model for microbiome therapeutics. *Exp. Mol. Med.* **52**, 1383–1396 (2020).
66. Chassaing B., Aitken J. D., Malleshappa M. & Vijay-Kumar M. Dextran sulfate sodium (DSS)-induced colitis in mice. *Curr. Protoc. Immunol.* **104**, 15.25.1–=15.25.14 (2014)
67. Carroll, I. M., Ringel-Kulka, T., Siddle, J. P., Klaenhammer, T. R. & Ringel, Y. Characterization of the fecal microbiota using high-throughput sequencing reveals a stable microbial community during storage. *PLoS ONE* **7**, e46953 (2012).
68. Sheng, Y., Mancino, V. & Birren, B. Transformation of Escherichia coli with large DNA molecules by electroporation. *Nucleic Acids Res* **23**, 1990–1996 (1995).
69. Michael, R. G. & Sambrook, J. *Molecular Cloning: A Laboratory Manual* 4th edn (CSHL Press, 2012).
70. Gibson, D. G. et al. Enzymatic assembly of DNA molecules up to several hundred kilobases. *Nat. Methods* **6**, 343–345 (2009).

Acknowledgements

The authors extend their gratitude to Dr. Tal Gefen, Ilan Oren, Roee Samuel, Ximing Li of the Technion-Israel Institute of Technology for their invaluable contributions. We acknowledge the financial support from the Israel Ministry of Science (Grant No. 3-17915), the Technion Human Health Initiative (THHI, Grant Agreement No. 1020837), and the Israel Innovation Authority (Grant No. 75699). This work was supported by the European Union's Horizon 2020 Research And Innovation Program FET-Open NEU-Chip (Grant Agreement No. 964877). This study also supported by the Rappaport Technion Integrated Cancer Center, the CIFAR (Grant No. FL-000969/FL-001245/FL-001381). We acknowledge the iGEM Team Technion Department of Biotechnology & Food Engineering for providing us the PLldR promoter (BBa_K822000) and appreciate the support of Technion's Lorry I. Lokey interdisciplinary Center for Life Sciences and Engineering. We also thank Timothy K.Lu laboratory for providing the plasmids pMM534 and pMM549, which contain the promoter $P_{L(HrtO)}$, *HrtR* and *ChuA* genes for the Heme-responsive strain.

Author contributions

R.H., V.K., and R.D. designed the study. R.H., V.K. and M.H. performed in vitro experiments and collected data. R.H., V.K. and R.Z. performed fecal sample experiments and collected data. R.D. and R.H. associated models and simulations. R.H., V.K., and R.D. wrote the manuscript. N.G.-Z. supervised the study and provided experimental assistance. All authors analyzed the data, discussed the results, and wrote the manuscript.

Competing interests

The authors declare no competing interests.

Additional information

Supplementary information The online version contains supplementary material available at https://doi.org/10.1038/s41467-025-58996-9.

Correspondence and requests for materials should be addressed to Ramez Daniel.

Peer review information *Nature Communications* thanks Iacopo Ruolo and the other, anonymous, reviewer(s) for their contribution to the peer review of this work. A peer review file is available.